# A Simple Free-Fold Test to Measure Bending Stiffness of Slender Soft Actuators

Gillian J. McDonald, Emmanuel Detournay, and Timothy M. Kowalewski

Abstract—A reliable estimate for bending stiffness is critical to many soft robot models when predicting everything from robotenvironment contact to buckling resistance. Current methods for predicting actuator bending stiffness rely on highly accurate knowledge of material characteristics, which are not trivial to obtain for composite actuators. Additionally, current models for fluidic actuators often depend on a pressure-independent bending stiffness despite pressure playing a non-negligible role in bending stiffness behavior. Methods to measure actuator stiffness often require costly instrumentation to measure or perturb the motions and forces required to measure actual bending stiffness. We introduce a simple free-fold test to empirically estimate the bending stiffness of slender soft actuators-pressurized or unpressurized and composite or homogeneous-which requires the measurement of one distance from a single image of a specific robot pose. The resulting model also shows that the change in actuator weight per unit length can be used to determine the dependence of bending stiffness on actuation pressure.

*Index Terms*—Soft robot applications, soft robot materials and design, soft sensors and actuators, medical robots and systems.

### I. INTRODUCTION

HEN modeling the behavior of soft robots, knowledge of the bending stiffness plays a critical role in everything from predicting the critical buckling force of an actuator to modeling the contact between a compliant, soft actuator and objects with which it comes into contact. Many soft robotic actuators are composed of multiple materials that help dictate their behavior upon actuation. Due to such composite nature, obtaining an accurate prediction of the bending stiffness, EI, of the overall structure is challenging and often requires both computationally expensive modeling (e.g. finite element) and in-depth knowledge of the material properties

Manuscript received March 13, 2021; accepted August 16, 2021. Date of publication September 24, 2021; date of current version October 7, 2021. This letter was recommended for publication by Associate Editor Prof. Robert MacCurdy and Editor Prof. Kyu-Jin Cho upon evaluation of the reviewers' comments. This work was supported in part by the National Science Foundation Emerging Frontiers in Research and Innovation (EFRI) C3 SoRo Program, in part by the National Science Foundation Graduate Research Fellowship Program under Grant 00039202, and in part by the Institute for Engineering in Medicine (IEM). (Corresponding author: Gillian J. McDonald.)

Gillian J. McDonald is with the Mechanical Engineering, University of Minnesota, Minneapolis, MN 55455 USA (e-mail: mcdo0658@umn.edu).

Emmanuel Detournay is with the Faculty of the Department of Civil, Environmental, and Geo-Engineering, University of Minnesota, Minneapolis, MN 55455 USA (e-mail: detou001@umn.edu).

Timothy M. Kowalewski is with the Faculty of the Mechanical Engineering Department, University of Minnesota, Minneapolis, MN 55455 USA (e-mail: timk@umn.edu).

Digital Object Identifier 10.1109/LRA.2021.3114960

of the actuator. Additionally, describing the bending stiffness becomes even more difficult for fluid-powered soft robots because of the effect that internal actuation pressure has on robot behavior.

In 1930, Peirce introduced the concept of a free-fold test approach to determine the bending rigidity and bending length for fabric sheets [1]. The free-fold test describes how a long sheet of material can be folded back on itself and, when released, the sheet forms a loop. The bending stiffness of the sheet can be deduced from the height of the loop and the weight per unit length of the sheet. The approach was later explored by others, including Stuart and Baird, Lloyd *et al.*, Wang, Mahadevan and Keller, Zhou and Gosh, Cassidy *et al.*, and Plaut ([2]–[9]) but has been utilized mainly by the textile research community.

Although various groups have studied how the stiffness of soft robots can be controlled, no simple method for determining the bending stiffness of slender, fluid-powered soft robots as a function of pressure exists—despite bending stiffness playing a critical role in many aspects of soft robot modeling. Blanc et al. provide a comprehensive literature review of flexible medical devices with controllable stiffness, including fluid-based solutions in soft robotic joints, but do not discuss bending stiffness models [10]. One article cited by Blanc et al. compares artificial actuators to muscle and emphasizes the importance of stiffening as a mechanical characteristic, but does not provide a stiffening model [11]. Others have experimentally measured bending stiffness of soft actuators, commonly using force and displacement sensors [12]–[14]. Alici et al. highlight the difficulty of estimating the stiffness of composite bending actuators using traditional tensile tests, so instead use an equation assuming the actuator's bending and blocking force behavior are known [15].

Specific to fiber-reinforced McKibben actuators, Tondu, Chou and Hannaford, and Thomalla and Van de Ven provide in-depth analyses for the strain and force behavior of McKibben actuators as functions of pressure [16]–[18]. Additionally, Van den Horn and Kuipers modeled the stresses and strains that develop in steel-braided flexible tubes as a result of internal pressure [19]. However, each of the models require knowledge of the material properties like Poisson's ratio and are not generalized to describe the bending stiffness of flexible tubes with multiple composite layers.

Outside of soft robotics, others have explored the effect of internal pressure on pipes and tubes using finite element methods. Catinaccio explored the behavior of straight, both uniform and composite laminate pipes subject to internal pressure and in-plane bending [20]. Teng *et al.* examine the deformation

2377-3766 © 2021 IEEE. Personal use is permitted, but republication/redistribution requires IEEE permission. See https://www.ieee.org/publications/rights/index.html for more information.

behavior of thin-walled tubes under internal pressure and combined bending, showing that pressure enhances bending stiffness by preventing ovalization [21]. Although these works provide insight as to how pressure combats bending for uniform pipes and tubes, they both required finite element modeling and did not derive an explicit relationship between bending stiffness and pressure.

This work provides two core contributions:

- The introduction of the free-fold test for slender soft robots to provide an empirical estimate of actuator bending stiffness, regardless of whether the actuator is uniform or composite, using straightforward experimentation.
- 2) An investigation of the factors contributing to the dependence of soft actuator bending stiffness on actuation pressure, presented using three models, particularly for McKibben actuators or other actuators that do not undergo out-of-plane bending when pressurized.

When combined, the contributions of this work provide a comprehensive design tool for slender soft robots that can be used to determine how actuator stiffness is affected by actuation pressure, when the magnitude of this effect is negligible, and how each actuator design variable plays a role in the bending stiffness behavior.

#### II. METHODS

### A. Free-Fold Test

1) Existing Textile Model: The free-fold test method discussed in the Introduction and utilized by the textile research community states that bending stiffness, EI, can be determined using the height of the folded loop, where

$$EI = 1.342\omega h^3 \tag{1}$$

where  $\omega$  denotes the uniform weight per length, h denotes the height of the fold, and bending stiffness is a product of the elastic modulus, E, and area moment of inertia, I, as shown by Plaut [9]. The length of the sheet must be

$$\ell > 4.683 \sqrt[3]{\frac{EI}{\omega}} \tag{2}$$

as outlined by [5] and [9]. This specified length is necessary to conduct the free-fold test, but the value of EI determined from the free-fold test still holds for shorter sheets.

- 2) Conditions Necessary for Free-Fold Test: The free-fold test requires uniformity along the longitudinal axis. This holds for cross-sectional geometry, elastic modulus, E, area moment of inertia, I, and weight per unit length,  $\omega$ . Additionally, beam theory must be applicable and the actuator length used for the test must meet the conditions of (2) [22].
- 3) Free-Fold Test for Soft Actuators: One of the major contributions of this letter is to demonstrate the applicability of the free-fold test to slender soft actuators. The original textile free-fold model was intended for long strips of fabric of rectangular cross section. However, the free-fold test is applicable to more complicated cross-sectional geometries, like those found in many soft robotics actuators, so long as the assumption of uniformity along the *longitudinal* axis holds. An example of a

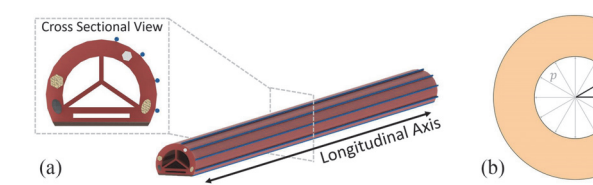


Fig. 1. (a) The free-fold test is applicable to actuators with non-uniform cross-sections, so long as the actuator is uniform along the longitudinal axis (Note: fiber wrapping is considered to meet the longitudinal axis uniformity condition). The hypothetical composite bending actuator shown meets these criteria (different colors imply different materials) while simple bellows or twisting actuators do not. (b) A simple, circular actuator cross section is used for the pressure-dependent bending stiffness models to provide a straightforward theoretical comparison to the empirical bending test. The actuator wall is an incompressible elastomer subject to internal pressure, p, and has pressure-dependent inner and outer radii,  $r_p$  and  $R_p$ , respectively.

cross section for which the free-fold test would still apply is shown in Fig. 1(a).

## B. Exploration of Pressure-Bending Stiffness Relationship for Incompressible Working Fluids

A secondary contribution of this letter is a determination of the variables that control the underlying dependence of bending stiffness on actuation pressure. To discover the driving variables, we first consider a tube-like, fluidic actuator with circular cross section comprised of incompressible elastomeric material, an internal pressure, p, a pressure-dependent inner radius,  $r_p$ , and a pressure-dependent outer radius,  $R_p$ , shown in Fig. 1(b) Each pressure-dependent variable is denoted by a subscript p for simplicity.

- 1) Assumptions for Pressure-Bending Stiffness Relationship: The models derived to explore the relationship between input pressure and bending stiffness assume the following:
  - Constant Elastic Modulus: The elastic modulus, E, is assumed to be known and constant across the pressure range of interest.
  - Uniformity Along the Longitudinal Axis: Like the original textile model, uniformity along the longitudinal axis must hold for cross-sectional geometry, elastic modulus, E, area moment of inertia, I, and weight per unit length,  $\omega$ .
  - Slender or "High Aspect Ratio" Geometry: The scope of this work focuses on slender or high aspect ratio soft actuators, where the overall actuator length is much greater than the actuator radius (or similar measurable parameter, such as cross-sectional width, for non-circular cross sections).
  - Fluid Incompressibility: The free-fold test applies to both incompressible and compressible working fluids (provided the working fluid weight is known). However, the theoretical equations shown in this section and Section II-C only consider incompressible working fluids to explore the relationship between pressure and bending stiffness. Rationale for this assumption is in the Appendix.
- 2) Weight Per Unit Length as Controlling Variable: To determine the dependence of bending stiffness on actuation pressure, we assume here that the actuator length does not change with pressure, which is equivalent to a plane strain assumption. This

assumption was motivated by experimental results for the fluidic actuators not reinforced by fibers discussed in later sections. We can describe the area moment of inertia,  $I_p$ , of the actuator as

$$I_{p} = \frac{\pi}{4} \left( R_{p}^{4} - r_{p}^{4} \right) = \frac{\pi}{4} \left( R_{p}^{2} - r_{p}^{2} \right) \left( R_{p}^{2} + r_{p}^{2} \right) \tag{3}$$

Since we assume the elastomer is incompressible,

$$\pi \left( R_n^2 - r_n^2 \right) = S \tag{4}$$

where S is a constant. We can describe the pressure-dependent radial displacement at the inner radius to be

$$u_p \simeq \frac{A}{2\pi r_0} \tag{5}$$

where A denotes the increase in area of the inner cross-section of the tube. Similarly, the radial displacement at the outer radius can be described as

$$U_p \simeq \frac{A}{2\pi R_0} \tag{6}$$

where A is the same in (5) and (6) on account of the incompressibility of the elastomer. The variation of moment of inertia can be expressed as

$$\Delta I_p = I_p - I_0 = \frac{S}{4} \left( R_p^2 + r_p^2 - R_0^2 - r_0^2 \right) \tag{7}$$

Since the radial displacement  $u_p = r_p - r_0$  and  $U_p = R_p - R_0$ , we can rewrite (7) as

$$\Delta I_p \simeq \frac{S}{4} \left( 2u_p r_0 + 2U_p R_0 \right) \simeq \frac{AS}{2\pi} \tag{8}$$

Let  $\Delta\omega_p$  denote the increase in weight per unit length of the actuator with pressurization. Then

$$A\rho = \Delta\omega_p \tag{9}$$

on account of the assumed incompressibility of the actuation fluid where  $\rho$  represents the fluid density. Hence,

$$\Delta I_p \simeq \frac{\Delta \omega_p S}{2\pi\rho} \tag{10}$$

From (10) we can conclude

$$\Delta I_p \sim \Delta \omega_p$$
 (11)

We assume the elastic modulus, E, stays constant throughout pressurization, meaning the change in bending stiffness with pressure,  $\Delta E I_p$ , is fully dependent on the change in moment of inertia,  $\Delta I_p$ , described by (11).

# C. Theoretical Model for Pressure-Dependent Bending Stiffness

The resulting equations from Section II-B show that the change in actuator bending stiffness as pressure increases,  $\Delta EI_p$ , is controlled by the measurable quantity  $\Delta \omega_p$  that corresponds to the pressure-dependent change in weight per unit length of the actuator, but a theoretical baseline for comparison is desirable.

Since the actuation fluid is assumed to be incompressible, the pressure increase is due to the compliance of the elastomeric actuator. We can treat the actuator as a thick-walled cylinder with open ends, internal pressure, p, initial inner radius,  $r_0$ , and initial outer radius,  $R_0$ . We can express the radial stress,  $\sigma_r$ , as

$$\sigma_r = \left(\frac{r_0^2 p}{R_0^2 - r_0^2}\right) - \left(\frac{r_0^2 R_0^2 p}{R_0^2 - r_0^2}\right) \frac{1}{b^2}$$
 (12)

where b represents the radius to a point of interest on the cylinder. We can express the tangential stress,  $\sigma_t$ , as

$$\sigma_t = \left(\frac{r_0^2 p}{R_0^2 - r^2}\right) + \left(\frac{r_0^2 R_0^2 p}{R_0^2 - r_0^2}\right) \frac{1}{b^2}$$
 (13)

Assuming now that the axial stress,  $\sigma_a$ , is zero, we can express the tangential strain,  $\varepsilon_t$ , in terms of radial and tangential stresses using Hooke's law

$$\varepsilon_t = \frac{(\sigma_t - \nu \sigma_r)}{E} \tag{14}$$

where Poisson's ratio,  $\nu$ , is 0.5 due to the assumed incompressibility of the elastomer [23]. We can express the radial displacement of the cylinder as

$$u_b = \varepsilon_t b \tag{15}$$

where the radial and tangential stresses are calculated at radius, b. The change in radius can be expressed in terms of internal pressure as

$$u_b = \left(\frac{1-\nu}{E}\right) \left(\frac{r_0^2 p}{R_0^2 - r_0^2}\right) b + \left(\frac{1+\nu}{E}\right) \left(\frac{r_0^2 R_0^2 p}{R_0^2 - r_0^2}\right) \frac{1}{b}$$
(16)

We can calculate the pressure-dependent inner and outer radii,  $r_p$  and  $R_p$ , respectively, by substituting  $b=r_0$  and  $b=R_0$  into the equation from (16), where

$$r_p = r_0 + u_{r_0} (17)$$

$$R_p = R_0 + u_{R_0} (18)$$

We can substitute (17) and (18) into (3) to find  $I_p$ . Finally, the theoretical bending stiffness can be expressed as

$$(EI)_p = EI_p \tag{19}$$

# D. Empirical Models for Pressure-Dependent Bending Stiffness

We present three empirical models (Weight-Based, Elastomer Volume, and McKibben) to estimate bending stiffness using measurable quantities (e.g. length, weight, strain, and outer diameter) as pressure changes.

The following variables are used throughout each of the models:

- $\omega_0$  initial overall actuator weight per unit length
- $\omega_p$  overall actuator weight per unit length
- $\omega_e$  weight per unit length of the elastomer and non-fluid materials
- $\ell_0$  initial actuator length
- $\ell_p$  pressurized actuator length
- $\rho$  density of the actuation fluid
- $R_0$  initial outer radius
- $R_p$  outer radius
- E elastic modulus
- $\theta_0$  initial, positive fiber wrap angle for McKibbens

1) Weight-Based Model: The result from (11) shows that the pressure-dependent relationship relies on variables that can be empirically measured in a simple manner, specifically  $\Delta\omega_p$ . Since we are interested in determining the pressure-dependent bending stiffness,  $EI_p$ , but the inner radius,  $r_p$ , is not empirically measurable using simple methods, we can verify (10) by deducing expressions for  $r_p$  and  $R_p$  from (5), (6), and (9) to get

$$r_p = \frac{\Delta\omega_p}{2\pi\rho r_0} + r_0 \tag{20}$$

$$R_p = \frac{\Delta\omega_p}{2\pi\rho R_0} + R_0 \tag{21}$$

The "Weight-Based" bending stiffness can be determined by substituting (20) and (21) into (3), then substituting the result into (19).

2) Elastomer Volume Model: The Elastomer Volume model determines bending stiffness based on the initial volume of the elastomer and other material properties. The model assumes the following variables are known or measurable:  $\omega_0$ ,  $\omega_e$ ,  $\ell_0$ ,  $\ell_p$ ,  $\rho$ ,  $R_0$ ,  $R_p$ , and E.

First, we determine the initial inner radius,  $r_0$ , by

$$r_0 = \sqrt{\frac{\omega_0 - \omega_e}{\pi \rho}} \tag{22}$$

The volume of the elastomer and non-fluid materials can be expressed as

$$v_e = \pi \ell_0 \left( R_0^2 - r_0^2 \right) \tag{23}$$

Since  $\ell_0$ ,  $\ell_p$ ,  $R_0$ ,  $R_p$ ,  $r_0$  are known and elastomer volume is conserved throughout actuation, we can determine the pressure-dependent inner radius,  $r_p$ , by

$$r_p = \sqrt{R_p^2 - \frac{\ell_0}{\ell_p} (R_0^2 - r_0^2)}$$
 (24)

Finally, the moment of inertia and bending stiffness can be found from (3) and (19).

3) McKibben Model: The McKibben model is specific to fiber-wrapped actuators and estimates the bending stiffness as a function of pressure assuming the following variables are known:  $\omega_0$ ,  $\omega_e$ ,  $\ell_0$ ,  $\ell_p$ ,  $\rho$ ,  $R_0$ , E, and  $\theta_0$ .

First, we adapt known equations from [18] to describe how the outer radius changes as a function of pressure using the known variables, where

$$R_p = \frac{R_0 \sqrt{1 - (1 + \varepsilon_p)^2 \cos^2 \theta_0}}{\sin \theta_0}$$
 (25)

where the axial strain,  $\varepsilon_p$ , is

$$\varepsilon_p = \frac{\ell_p - \ell_0}{\ell_0} \tag{26}$$

The wall thickness as a function of pressure,  $t_p$ , can be described by

$$t_p = R_p - \sqrt{R_p^2 - \frac{t_0(2R_0 - t_0)}{1 + \varepsilon_p}}$$
 (27)

TABLE I ACTUATORS TESTED USING FREE-FOLD TEST

Reference Name	Description	OD (mm)	ID (mm)
Baseline	Solid elastic rod; polyurethane	3.23	N/A
Small,			
Unwrapped	Natural rubber tube; no fiber- reinforcement	3.18	1.59
Large,			
Unwrapped	Natural rubber tube; no fiber- reinforcement	4.76	3.18
Small,			
Wrapped	Natural rubber tube; fiber-reinforced; dipped in polyurethane	3.99	1.59

where the initial wall thickness,  $t_0$ , is found by

$$t_0 = R_0 - r_0 (28)$$

and the initial inner radius is expressed as

$$r_0 = \sqrt{\frac{\omega_0 - \omega_e}{\pi \rho}} \tag{29}$$

We can then determine the inner radius as a function of pressure using

$$r_p = R_p - t_p \tag{30}$$

Finally, the moment of inertia and "Elastomer Volume Model" bending stiffness can be found from (3) and (19).

## E. Experiments

The goal of the experiments was three-fold. First, we sought to confirm that the fold test could be used as a simple, effective method for determining the bending stiffness of soft actuators regardless of whether they were constructed of uniform or composite materials. Second, we sought to validate (11) to approximately predict the change in bending stiffness with the change in weight per unit length. Third, we wanted to determine how both geometry and fiber-reinforcement affect the bending stiffness-pressure relationship.

The experiments were conducted using four actuator types describe in Table I. A visual comparison of each actuator is shown in Fig. 2. The elastic modulus, E, for the natural rubber tube (Kent Elastomer natural rubber latex tubing) was 1.31 MPa (190 psi) based on the data sheet provided by the supplier (latextubing.com) [24]. The Poisson's ratio for the natural rubber tube was assumed to be  $0.50 \pm 0.01$  [23]. The working fluid was water.

1) Free-Fold Test Process: Each free-fold test was conducted by tying five strands of thread (30 wt. 100% cotton, Coats) to the actuator so that the actuator could be suspended into a pre-release configuration (Fig. 3(a)). The actuator was placed between two panes of transparent acrylic to prevent out-of-plane deflection and the actuators were coated with talc free powder (Up&Up Talc Free Powder) to reduce friction developed between the actuator and acrylic. For all experiments aside

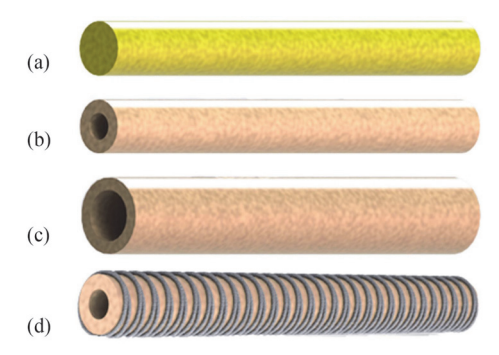


Fig. 2. Actuators tested experimentally using fold test: (a) Baseline actuator; a solid cross-section, elastic rod of polyurethane (Polytek 74-20). (b) Small, unwrapped actuator made from natural rubber tubing with 3.18 mm OD and 1.59 mm ID. (c) Large, unwrapped actuator made from natural rubber tubing with 4.76 mm OD and 3.18 mm ID. (d) Small, wrapped actuator made from natural rubber tubing, wrapped with 100%, 30 wt. cotton fibers, and dipped in polyurethane to secure the fibers in place (polyurethane dip layer not pictured), with 3.99 mm OD and 1.59 mm ID.

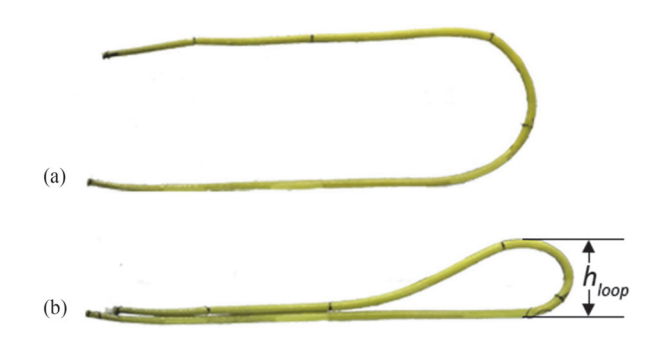


Fig. 3. (a) Example pre-release configuration with strands of thread used to suspend one half of the actuator. (b) Example post-release configuration with gravity forcing the actuator to form a free-fold loop.

from the baseline experiment, each actuator was pressurized to the appropriate pressure before being suspended into the pre-release configuration. Pressure data were collected at 10 Hz using a micro-controller (Teensy 3.5) connected to a pressure transducer (Honeywell TBPDANS030PGUCV) and load cell amplifier (SparkFun, HX711). With the actuator suspended into the pre-release configuration, all strands of thread were released at the same time and the actuator formed a post-release, free-fold loop (Fig. 3(b)). After the actuator was released, a static image was taken using a camera (iPhone 11 with Dual 12MP cameras) placed at a fixed distance from the test setup and at the same height as the actuator. This process was repeated five times for each actuator tested.

The full setup is shown in Fig. 4. The pixel-to-mm conversion ratio was calculated using an Augmented Reality University of Cordoba (ArUco) tag of known dimensions ( $25 \text{ mm} \times 25 \text{ mm}$ ) fixed to the test stand [25], [26].

Before each free-fold test was conducted, each actuator was measured for initial length, initial weight of the actuator without fluid, and the weight of the actuator over the pressure range of 0 to 172.37 kPa (0-25 psi) in 34.47 kPa (5 psi) increments. The weight measurements (performed using a 0.1 g resolution Smart Weigh Digital Pro Pocket Scale) properly accounted for

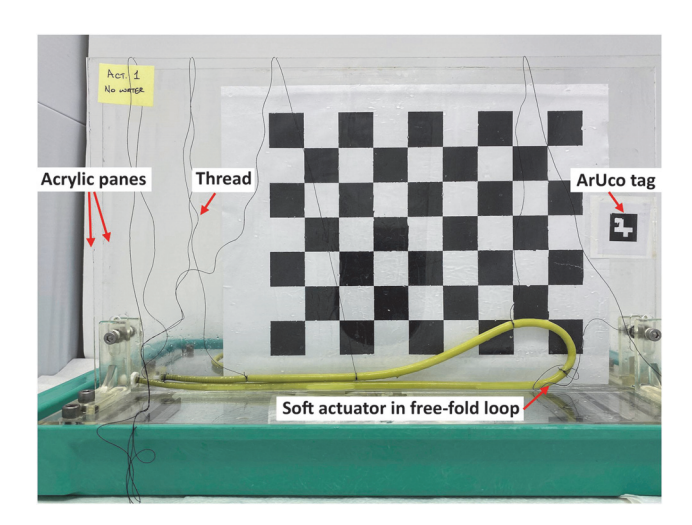


Fig. 4. Experimental test stand used for all free-fold tests. Actuators were placed between two panes of acrylic, suspended into the pre-release configuration using thread, and released to form the free-fold loop shown. Note: to adequately capture the details of the test stand, the camera angle used in this figure is not the same as was used to capture images of each free-fold test.

TABLE II ACTUATOR DIMENSIONS FOR BASELINE FREE-FOLD TEST

Actuator	OD (mm)	Length (mm)
1	3.25	614
2	3.20	462
3	3.24	612
4	3.23	612
Avg	$3.23 \pm 0.02$	575

the weight of the powder, thread, and barbed caps and fittings. Additionally, the relationship between actuator length and pressure, as well as outer radius and pressure, were determined using static images where the actuator was placed on a flat surface and pressurized over the pressure range in 34.47 kPa (5 psi) increments. A static image (top-view) was taken at each pressure increment and the actuator length and outer diameter were measured in post-processing using a pixel-to-mm conversion (using the "Measure Distance" tool in MATLAB; average of 9.7 pixels-per-mm).

- 2) Baseline: A baseline experiment was conducted using solid-bodied actuators, shown in Fig. 2 (a), to confirm that the free-fold test can be used to characterize the bending stiffness of soft actuators despite being originally used to characterize textile strips. Four solid-bodied polyurethane (Polytek 74-20) actuators were fabricated using a custom mold and injection process with dimensions shown in Table II. The actuators were tested using the process outlined in Section II-E1.
- 3) Pressurized Actuators: Two of each type of actuator listed in Table I, excluding the baseline actuators, were tested using the process outlined in Section II-E1. Data were recorded for the initial length and weight of each actuator, as well as strain and outer radius as functions of pressure. It should be noted that the large, unwrapped actuator (Table I) was tested over a smaller pressure range of 0 to 137.90 kPa (0 to 20 psi) to ensure the actuator did not burst or bulge.

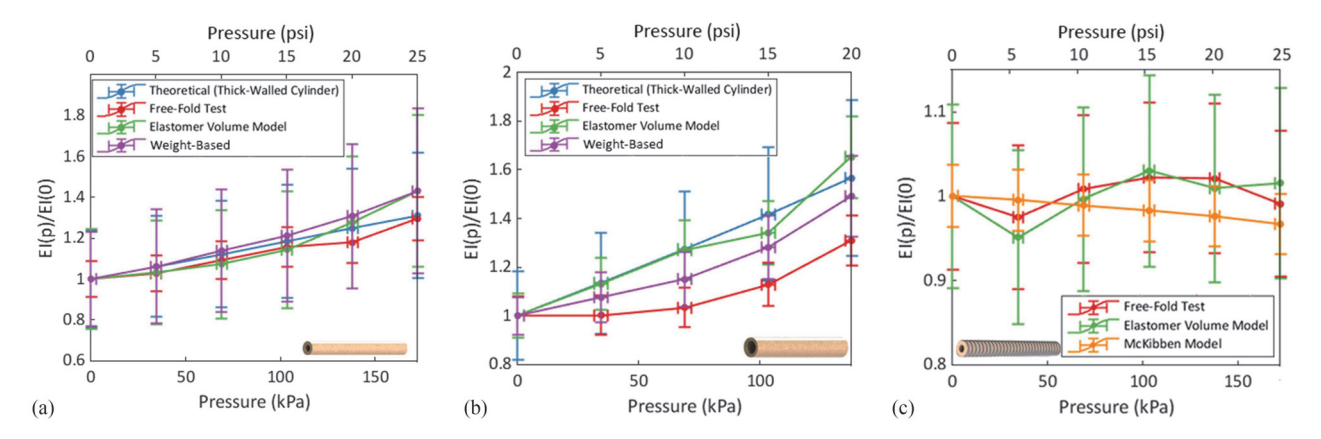


Fig. 5. The ratio of pressure-dependent to initial bending stiffness, showing consensus among applicable models, for: (a) Small, Unwrapped Actuator, (b) Large, Unwrapped Actuator, and (c) Small, Fiber-Wrapped Actuator. Pressure shown is gauge pressure. The x-error bars were determined by the overall variation ( $\pm 2.76$  kPa) in pressure observed throughout the free-fold tests. The y-error bars were determined using error propagation based on the measurement error of each of the known quantities described in Section II-A.

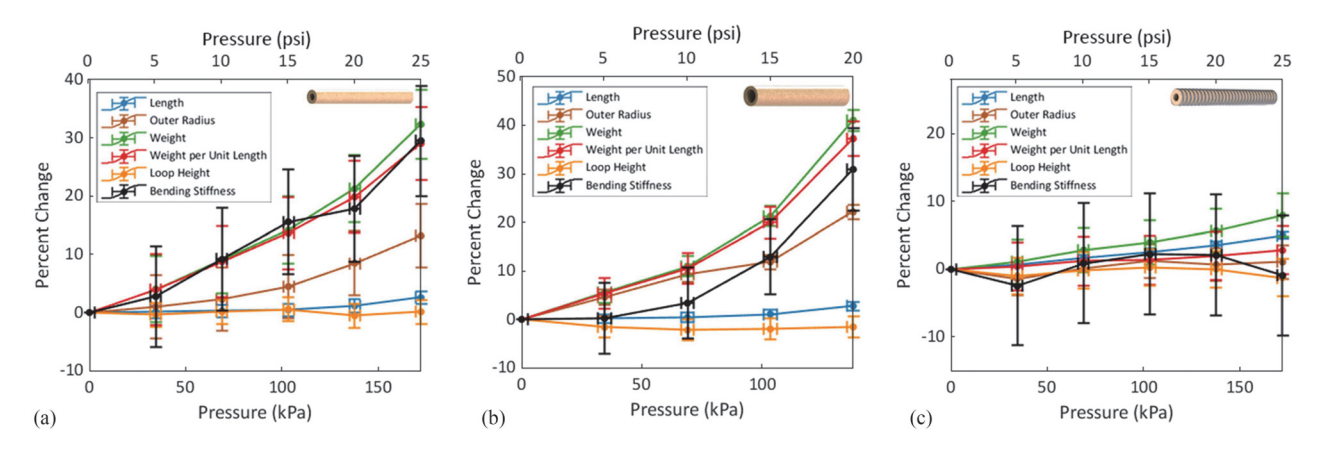


Fig. 6. The percent change in experimental variables with increasing pressure is shown for: (a) Small, Unwrapped Actuator, (b) Large, Unwrapped Actuator, (c) Small, Fiber-Wrapped Actuator. Pressure shown is gauge pressure. The x-error bars were determined by the overall variation ( $\pm 2.76$  kPa) in pressure observed throughout the free-fold tests. The y-error bars were determined using error propagation based on the measurement error of each of the known quantities described in Section II-A.

#### III. RESULTS

## A. Experimental Results

1) Baseline: The average loop height of the four baseline actuators was 29.97 mm and the average weight per unit length was  $7.77 \times 10^{-5}$  N/mm. This resulted in an average bending stiffness of 2.51 Nmm². Extracting the elastic modulus from the bending stiffness using the known geometry from Table II resulted in an average extracted modulus of  $0.49 \pm 0.11$  N/mm². We compared this value to the elastic modulus for the same polyurethane (Polytek 74-20) found using tensile tests conducted on dog bone samples (2 mm thick, 5 mm wide, 40 mm long) using an Instron machine, where the average tensile test modulus (N = 3 samples) was  $0.46 \pm 0.03$  N/mm². Thus, the percent difference between the elastic modulus extracted from the free-fold test and the elastic modulus determined from tensile tests was 6.86%.

2) Pressurized Actuators: The relationship between the experimental and modeled bending stiffness as a function of

pressure, from Section II-D, is shown in Fig. 5 for each of the pressurized actuator types. The contribution of each experimental variable to the percent change in the experimental bending stiffness is shown in Fig. 6 for each of the pressurized actuator types.

## IV. DISCUSSION

#### A. Baseline

The baseline experiment conducted using a solid-cross section elastic rod confirmed that despite being originally formulated for ribbon-like textiles, the free-fold test is an adequate approach to estimate the material properties of the soft actuators discussed throughout this letter given that the percent difference between the elastic modulus found from tensile tests and the free-fold test was 6.86%. This is on the order of the smallest percent difference between the elastic moduli of the three dog bone samples of the Polytek 74-20 polyurethane (6.73%) found using the Instron machine—with the largest percent difference between the three

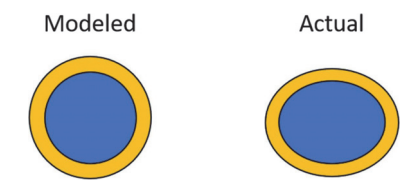


Fig. 7. One potential explanation for the discrepancy between experimental and modeled behavior for the large, unwrapped actuator is ovalization of the cross-section.

samples being 13.46%. We observed that the free-fold test resulted in a larger variation in measurement as compared to the tensile tests, although this was expected because the tensile tests were conducted on dog bone samples using an industrial Instron machine specifically designed for the purpose.

It is also critical to emphasize that one of the greatest benefits of the free-fold test, aside from its simplicity, is to characterize the bending stiffness of composite soft actuators as well as fluid-filled actuators. With this in mind, the purpose of the baseline experiment was to confirm that the free-fold test is valid for elastica beyond ribbon-like textiles rather than prove the accuracy of the free-fold test in extracting the elastic modulus of a homogeneous material.

### B. Pressurized Actuators

1) Pressure-Dependent Bending Stiffness: The experimental results for the pressurized actuators provided insight on how bending stiffness changes with pressure, as well as how the change is dictated by the cross-sectional geometry of the actuators and whether the actuator is fiber-reinforced. As can be seen from Figs. 5 (a) and 5 (b), bending stiffness increased with pressure for actuators that were not fiber-reinforced. The results showed that the proposed models were in agreement with the experiment for the small, unwrapped actuator. An improvement in the equipment used to measure each variable that contributes to EI would help to reduce the amount of error shown for both the proposed models and free-fold test experiment.

We noticed a greater difference between the experimental bending stiffness and the models for the large, unwrapped actuator. One possible explanation for this is measurement error and the high sensitivity of the experimental bending stiffness value to the measured loop height (i.e.  $h^3$  term). A second possible explanation is that when the ratio between inner and outer radii is large enough, the actuator cross section has a tendency to ovalize due to gravity when resting on a flat surface (Fig. 7). This ovalization would result in a slightly smaller loop height measurement, which would greatly affect EI due to its sensitivity to h. This ovalization would also cause a reduction in I, which is directly related to EI. Interestingly, the actuator geometry with a larger inner radius to outer radius ratio (i.e. large, unwrapped actuator) appeared to display an exponential relationship between bending stiffness and pressure.

Finally, a comparison between the actuators of similar geometry but differing fiber-reinforcement (e.g. small, unwrapped vs. small, wrapped) as shown in Figs. 5 (a) and 5 (c), showed that the presence of fibers significantly affects the bending stiffness and

pressure relationship. Fig. 5(c) showed that the bending stiffness does not increase with pressure when the actuator is reinforced with fibers. This is because the fibers restrict expansion of the outer radius,  $R_p$ , while the pressure causes an increase in the inner radius,  $r_p$ , and axial extension. This leads to a decrease in I and thus, EI. Although the McKibben model predicted a negative correlation between EI and p, the free-fold test and elastomer volume model results did not display any correlation.

2) Effect of Actuator Parameters on Bending Stiffness: We gained a stronger understanding of why bending stiffness changes—or does not change—with pressure by investigating the variable change with pressure, as shown in Fig. 6. The results showed that for the unwrapped case, specifically, the percent change in bending stiffness to pressure relationship followed most closely to the pressure-dependent relationships for outer radius, weight, and weight per unit length. Although the percent change in loop height as pressure increased followed a similar trend to bending stiffness, the percent change in loop height was smaller than that of bending stiffness. Again, the high sensitivity of the experimental bending stiffness value to the measured loop height (i.e.  $h^3$  term) could be an explanation for this, meaning that although the loop height has a smaller percent change over the range of pressures, a small change in h leads to a larger change in EI. The variable breakdown for the small, wrapped (McKibben) actuator showed that the fiber-reinforcement restricted the outer radius from increasing while promoting axial strain. The restriction of the outer radius impacted the moment of inertia for the actuator and thus, the bending stiffness.

## V. CONCLUSION

In this work, we presented a model to determine the bending stiffness of soft actuators, composite or homogeneous, using the free-fold test. Additionally, we showed that the change in weight per unit length controls the underlying dependence of bending stiffness on actuation pressure, which is easily measurable in soft robotics. Finally, we provided three models that predict the relationship between actuator bending stiffness and pressure for fluid-filled soft actuators, which is not incorporated into existing work such as [9].

Our models and experiments also shed light on the roles that cross-sectional actuator geometry and fiber-reinforcement play in the bending stiffness-pressure relationship. We provided an analysis of the specific contributions of each variable to the overall bending stiffness behavior, which elucidates the measurements and design variables that are most impactful to bending stiffness.

Overall, this work contributes a design tool and insight to the soft robotics community as to how fluid-powered soft robot bending stiffness is affected by pressure. Furthermore, our work outlines straightforward and manageable experiments that can be conducted without the need for computationally expensive finite element modeling and detailed knowledge of the structure and materials within composite actuators. Although this work touched briefly on modeling radial strains as a function of pressure without the need for empirical measurements (Thick-Walled Cylinder Model, Section II-C), the benefit of our proposed models is that they do not require in-depth knowledge of the actuator's material properties to provide a bending stiffness estimate.

The proposed work could be extended to actuators that contain composite components beyond fibers (e.g. strain limiting layers, rigid elements, etc.). Finally, a comparison between the free-fold test and other tests, such as a cantilever elastica under its own weight or a four-point flexural test, could be used to further explore the pressure-dependent bending stiffness of elastica [27]–[29].

## Appendix

## ASSUMPTION OF INCOMPRESSIBILITY

As noted in Section II-B1, the models discussed throughout this work assume working fluid incompressibility and use a pressure-dependent change in weight per unit length,  $\omega_p$ , to describe deformation of the elastomer and thus the pressure-dependency of bending stiffness. For purposes of providing straightforward, pressure-dependent models to compare with the empirical free-fold test results, this letter assumes the soft actuator's cross section is circular and the working fluid is water (although this simple cross section is not a limitation of the free-fold test, as described in Section II-A3).

To show that the assumption of working fluid incompressibility can be made, let  $\Delta v_f$  represent the change of fluid volume within a unit slice of the actuator's circular cross section, where

$$\Delta v_f = \frac{\Delta \omega_f}{\rho_f} \tag{31}$$

where  $\omega_f$  and  $\rho_f$  represent the weight per unit length and density of the fluid, respectively. In general,  $\Delta v_f$  is balanced by the compression of the fluid,  $\Delta v_c$ , and the deformation of the elastomer,  $\Delta v_e$ . That is,

$$\Delta v_f = \Delta v_c + \Delta v_e \tag{32}$$

where  $\Delta v_c = \frac{\pi r_0^2 p}{K_f}$  and  $\Delta v_c = 2\pi r_0 u_p$ , where  $u_p$  is the radial displacement at  $r = r_p$ . Assuming a "small" thickness of the elastomer ring (i.e.  $\delta << 1$ ) where  $\delta = \frac{R_0 - r_0}{R_0 + r_0}$ . It can readily be shown that  $u_p = \frac{p}{E} \frac{r_0}{2\delta}$ . Hence,

$$\Delta v_f = \frac{\pi r_0^2}{E\delta} p \left[ 1 + \frac{E\delta}{K_f} \right] \tag{33}$$

From this, the relative influence of the fluid compressibility and the actuator compliance on the fluid pressure increase to an increase of the fluid mass in the actuator is legislated by  $\beta = \frac{E\delta}{K_s}$ .

Hence, if  $\beta << 1$ , the pressure increase depends on E and not on  $K_f$ , and if  $\beta >> 1$  the reverse is true. For the experiments with the unwrapped actuators reported in this work,  $\beta \approx 10^{-3}$ , implying the fluid can be considered as incompressible, and the pressure is then proportional to E.

## REFERENCES

- [1] F. T. Peirce, "The "handle" of cloth as a measurable quantity," *J. Textile Inst. Trans.*, vol. 21, no. 9, pp. T 377–T416, Jan. 1930.
- [2] I. Stuart, "A loop test for bending length and rigidity," J. Appl. Phys., vol. 17, pp. 1215–1220, 1966.

- [3] I. Stuart and K. Baird, "A new test for bending length," *Textile Res. J.*, vol. 36, no. 1, pp. 91–93, 1966.
- [4] D. W. Lloyd, W. J. Shanahan, and M. Konopasek, "The folding of heavy fabric sheets," *Int. J. Mech. Sci.*, vol. 20, no. 8, pp. 521–527, Jan. 1978.
- [5] C. Y. Wang, "Post-buckling of horizontal heavy elastic sheet," J. Eng. Mech., vol. 110, no. 6, pp. 871–878, Jun. 1984.
- [6] L. Mahadevan and J. B. Keller, "Periodic folding of thin sheets," Soc. Ind. Appl. Math., vol. 41, no. 1, pp. 115–131, 1999.
- [7] N. Zhou and T. Ghosh, "On-line measurement of fabric bending behavior," *Textile Res. J.*, vol. 68, no. 7, pp. 533–542, Jul. 1998.
- [8] T. Cassidy, C. Cassidy, S. Cassie, and M. Arkison, "The stiffness of knitted fabrics: A new approach to the measurement of bending - part 1: Development," vol. 3, no. 5, pp. 14–19, May 1991.
- [9] R. H. Plaut, "Formulas to determine fabric bending rigidity from simple tests," *Textile Res. J.*, vol. 85, no. 8, pp. 884–894, 2015.
- [10] L. Blanc, A. Delchambre, and P. Lambert, "Flexible medical devices: Review of controllable stiffness solutions," *Actuators*, vol. 6, no. 3, pp. 1–31, 2017.
- [11] I. W. Hunter and S. Lafontaine, "A comparison of muscle with artificial actuators," in *Proc. IEEE Tech. Dig. IEEE Solid-State Sensor Actuator Workshop*, 1992, pp. 178–185.
- [12] I. Must, E. Sinibaldi, and B. Mazzolai, "A variable-stiffness tendril-like soft robot based on reversible osmotic actuation," *Nat. Commun.*, vol. 10, no. 1, pp. 1–8, 2019.
- [13] A. Kandhari, Y. Huang, K. A. Daltorio, H. J. Chiel, and R. D. Quinn, "Body stiffness in orthogonal directions oppositely affects worm-like robot turning and straight-line locomotion," *Bioinspiration Biomimetics*, vol. 13, no. 2, 2018, Art. no. 026003.
- [14] S. Zhu, Z. Guo, and C. Ji, "Experimental study on bending stiffness of a soft pneumatic filament-polymer actuator," in *Proc. ACM Int. Conf. Proc.*, 2019, pp. 616–620.
- [15] G. Alici, T. Canty, R. Mutlu, W. Hu, and V. Sencadas, "Modeling and experimental evaluation of bending behavior of soft pneumatic actuators made of discrete actuation chambers," *Soft Robot.*, vol. 5, no. 1, pp. 24–35, 2018.
- [16] B. Tondu, "Modelling of the McKibben artificial muscle: A review," J. Intell. Mater. Syst. Struct., vol. 23, no. 3, pp. 225–253, 2012.
- [17] C. P. Chou and B. Hannaford, "Measurement and modeling of McKibben pneumatic artificial muscles," *IEEE Trans. Robot. Autom.*, vol. 12, no. 1, pp. 90–102, Feb. 1996.
- [18] S. D. Thomalla and J. D. Van De Ven, "Modeling and implementation of the McKibben actuator in hydraulic systems," *IEEE Trans. Robot.*, vol. 34, no. 6, pp. 1593–1602, Dec. 2018.
- [19] B. Van den Horn and M. Kuipers, "Strength and stiffness of a reinforced flexible hose," Appl. Sci. Res., vol. 45, no. 3, pp. 251–281, 1988.
- [20] A. Catinaccio, "Pipes under internal pressure and bending," Cern, Tech. Rep., 2009.
- [21] B. G. Teng, L. Hu, and S. J. Yuan, "Deformation behavior of thin-walled tube bending with internal pressure, "Rev. Adv. Mater. Sci., vol. 33, no. 5, pp. 436–441, 2013.
- [22] H. Wang and Q-H. Qin, "Mechanics of solids and structures," in *Methods of Fundamental Solutions in Solid Mechanics*, Cambridge: Elsevier, 2019, ch. 2, pp. 53–89.
- [23] Polymer Properties Database, "Typical Poisson's ratios of polymers at room temperature," [Online]. Available: https://polymerdatabase.com/ polymerphysics/PoissonTable.html. [Accessed 2021]
- [24] Latex-Tubing.com, "Technical specifications," [Online]. Available: http://www.latex-tubing.com/Technical.html. [Accessed 2021].
- [25] F. J. Romero-Ramirez, R. Muñoz-Salinas, and R. Medina-Carnicer, "Speeded up detection of squared fiducial markers," *Image Vis. Comput.*, vol. 76, pp. 38–47, 2018.
- [26] S. Garrido-Jurado, R. Muñoz-Salinas, F. J. Madrid-Cuevas, and R. Medina-Carnicer, "Generation of fiducial marker dictionaries using mixed integer linear programming," *Pattern Recognit.*, vol. 51, pp. 481–491, 2016.
- [27] "Corrugated fibreboards and boards Bending stiffness Four-point method, Scandinavian Pulp, Paper and Board Testing Committee, SCAN-test Method 65:91, 1991.
- [28] Y. Wyser, C. Pelletier, and J. Lange, "Predicting and determining the bending stiffness of thin films and laminates," *Packag. Technol. Sci.*, vol. 14, no. 3, pp. 97–108, 2001.
- [29] R. H. Plaut, "Determining effective bending stiffness of fabrics and other materials from tests involving an added weight," *Textile Res. J.*, vol. 90, no. 1, pp. 101–109, 2020.